

Fooling Polarization-based Vision using Locally Controllable Polarizing Projection

Zhuoxiao Li[†] Zhihang Zhong[†] Shohei Nobuhara[‡] Ko Nishino[‡] Yinqiang Zheng^{†*}
[†]The University of Tokyo [‡]Kyoto University

Abstract

Polarization is a fundamental property of light that encodes abundant information regarding surface shape, material, illumination and viewing geometry. The computer vision community has witnessed a blossom of polarization-based vision applications, such as reflection removal, shape-from-polarization, transparent object segmentation and color constancy, partially due to the emergence of single-chip mono/color polarization sensors that make polarization data acquisition easier than ever. However, is polarization-based vision vulnerable to adversarial attacks? If so, is that possible to realize these adversarial attacks in the physical world, without being perceived by human eyes? In this paper, we warn the community of the vulnerability of polarization-based vision, which can be more serious than RGB-based vision. By adapting a commercial LCD projector, we achieve locally controllable polarizing projection, which is successfully utilized to fool state-of-the-art polarization-based vision algorithms for glass segmentation and color constancy. Compared with existing physical attacks on RGB-based vision, which always suffer from the trade-off between attack efficacy and eye conceivability, the adversarial attackers based on polarizing projection are contact-free and visually imperceptible, since naked human eyes can rarely perceive the difference of viciously manipulated polarizing light and ordinary illumination. This poses unprecedented risks on polarization-based vision, both in the monochromatic and trichromatic domain, for which due attentions should be paid and counter measures be considered.

1. Introduction

Even if the frequency of light lies in the visible range, its polarization status can hardly be perceived by human eyes. Fortunately, a variety of imaging devices have been developed, which allow to utilize rich scene information encoded in polarization, regarding geometry, material, il-

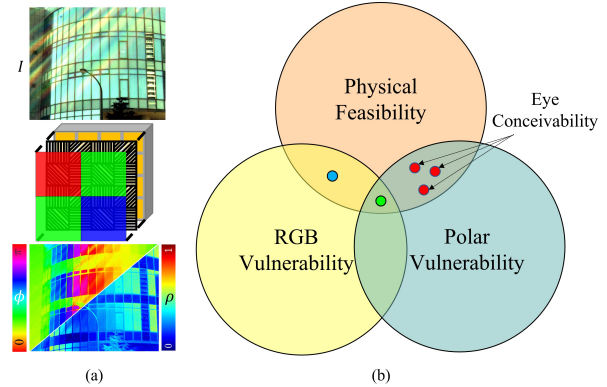


Figure 1. (a) Single-chip color polarization sensor can capture trichromatic image, angle of linear polarization (AoLP), and degree of linear polarization (DoLP) within one shot. (b) Our proposed physical attackers are based on polarizing projection, which is naturally conceivable to human eyes, thus can bypass the trade-off between attack efficacy and eye conceivability in fooling RGB-based vision.

lumination and light transportation. The emergence of single-chip mono/color polarization sensors has made polarization data acquisition easier, leading to a blossom of polarization-based vision applications, such as reflection removal [23], shape-from-polarization [10, 13], surface defects detection [25], color constancy [30], transparent object detection and segmentation [27]. Figure 1 (a) shows the capabilities of a single-chip color polarization sensor in capturing trichromatic image I , angle of linear polarization (AoLP) ϕ , and degree of linear polarization (DoLP) ρ , with one shot. Given the prevalence of polarization-based vision, it is astonishing that its vulnerability has never been formally explored in the computer vision community.

The vulnerability of RGB-based deep vision models is firstly reported in [32], with various extensions in minimizing perturbation magnitude, maximizing success rate of attack, retrieving universal adversarial attackers, and so on [1, 2]. Stepping beyond the digital space, more recent researches focus on studying the vulnerability of RGB-based vision models in the physically feasible space, while minimizing the level of offensiveness to human eyes (blue

*Corresponding author

point in Figure 1(b)), by using printed attack patterns on papers [22, 5, 20], clothes [36], or perturbations projected by projectors [14], and attacks created by laser beams [11] and shadows [40]. In principle, physical adversarial attack can be more catastrophic, since there is no need to hack the input image or the deployed model as digital attack requires. However, it is extremely hard to find a physical attacker that is both effective and imperceptible, since RGB cameras by design are mimicking human eyes, and a physically feasible attack that is invisible to eyes will not be captured by the camera as well.

Given that polarization and color represent two distinct dimensions of light, and polarization is usually introduced as a complementary modality to assist RGB-based vision, one might believe that, polarization-based vision, especially when coupled with the RGB modality, should be safer and harder to be attacked in the physical world, as the green dot in Figure 1(b) illustrates. In this paper, we show that this speculation is ungrounded by proposing a novel yet simple implementation of locally controllable polarizing projection. Since human eyes have no sensitivity to polarization, the most stringent restriction on eye conceivability in attacking RGB-based vision is naturally bypassed. This allows us to explore the vulnerability space of polarization-based vision more flexibly, within in the broad feasible space that the projector can realize (red dots in Figure 1(b)).

Inspired by the operating principle of Liquid Crystal Display (LCD) panels in monitors and projectors, we have recognized that the polarization status of light emitted from each liquid crystal cell can be independently controlled, after removing the front polarization film attached onto the LCD panel. Since human eyes can not perceive polarization status, the projected light looks uniformly white, even if the projection pattern has colors and textures, and the polarization status of light has been adjusted accordingly by LCD. In contrast, polarization cameras can record the programmed polarizing projection, and the behaviors of vision algorithms based on such information might be manipulated.

We have verified the feasibility of fooling polarization-based vision for two representative tasks, including (i) reducing accuracy of RGB-polar based glass segmentation [27] via whitebox attack; (ii) misleading the latest color constancy algorithm on the basis of trichromatic color and polarization [30] with complete blackbox attack. We hope this study can arouse attention on the potential security risks of utilizing polarization and trigger further researches on the defense side.

2. Related Work

2.1. Adversarial Attacks on RGB-based Vision

While the state-of-the-art deep neural networks are capable of achieving incredible performance in various scene understanding tasks, recent researches [22, 32] revealed their striking vulnerability that very mild modifications to the input images can deceive advanced classifiers with high confidence. The adversarial examples are generated through optimization processes by maximizing classification error of a targeted model. In digital world, on the premise of direct access to the targeted model, an adversarial example can be derived by one or multiple steps of perturbation following negative gradient directions, including classic Fast Gradient Sign Method (FGSM) [15], the Basic Iterative Method (BIM) [15], and the Projected Gradient Descent (PGD) [26] for efficient and transferable adversarial attacks. Their perturbations are bounded with a small norm-ball $L_p < \epsilon$, normally $p = 2$ or ∞ , or minimized with a joint adversarial loss [8], to craft a quasi-imperceptible example to human eyes. [29, 16] unveil the existence of a universal adversarial perturbation to a target model and it can achieve high transferability across different neural networks.

Digital attacks assume they can hijack the prediction system to directly feed adversarial examples into the targeted model. Considering that this requirement is usually impractical, other researches try to realize adversarial attacks by inserting perturbations into the physical world. [22] shows adversarial examples printed on papers are partly effective to fool DNN classifiers. However, because of the discrepancy between the designed attacker in the digital space and the physical attacker recorded by the camera, a key task is to retrieve robust adversarial examples that can be faithfully realized. [20] approximates the full digital-to-physical transformation to search perturbations in a simulated parallel world. To deal with the wide range of diversities in real world scenarios, e.g. view points, illuminations, and noises, [5] gets a distribution of transformations involved in the optimization procedure, including rescaling, rotation (in 2D or 3D), translation of image, and so on.

However, former small perturbations are too subtle to be captured by cameras in the wild. Therefore, recent physical-world adversarial attack methods attempt to generate strong but stealthy perturbations in real world. For example, stickers and graffiti type perturbations are attached on targeted object, e.g. a road sign, to achieve targeted misclassification from arbitrary view points. Wearable attack perturbations like clothes [37] and eye-glasses [31] are capable of fooling detection systems with improved stealthiness. Moreover, laser beams [11], shadows [40], and projection [14] are utilized to craft attack perturbations in physical world without touching target objects. We refer readers to [35] for thor-

ough literature reviews on physical adversarial attack. All these researches on physical adversarial attack have to make a trade-off between attack efficacy and eye conceivability.

2.2. Polarization-based Vision

Polarization has been utilized in various vision tasks for many years, which is further boosted recently due to the emergence of single-chip polarimetric imaging sensor that provides chromatic and polarimetric information in a single shot. Polarization cues are highly related to surface geometry and material property. Thus, it is introduced to assist conventional stereo vision approaches, i.e. multi-view stereo [9, 38], binocular stereo [13], and photometric stereo [34]. Besides, polarized specular and diffuse reflection have distinct properties, which make it also popular in inverse rendering by formulating the physics-based rendering equation with polarimetric Bidirectional Reflection Distribution Function (pBRDF) model [7, 19, 39]. With learned shading and polarization priors, DNNs can restore more detailed geometries [6, 24] and SVBRDF [10] with a single shot. Moreover, polarimetric imaging is capable of capturing polarization cues of transparent objects, which explains its extraordinary superiority in dealing with transparent objects in glass segmentation [27], transparent object shape estimation [28], and reflection removal [23]. Color constancy is challenging in the RGB domain, and it is shown that polarization can benefit color constancy, especially in poorly illuminated conditions [30].

Wider applications of polarization in the near future can be expected, yet we would like to warn of the potential vulnerability of polarization-based vision, which might be more serious than that of RGB-based vision, since the adversarial attackers can be physically realized by using a modified LCD projector and human eyes can not differentiate maliciously manipulated polarizing light from normal illumination.

2.3. Projectors and Their Applications

Projectors are widespread display devices, whose modulation mechanism of light intensity is either based on digital micromirror device (DMD) widely used in digital light processing (DLP) projectors or liquid crystal polarization adopted by LCD projectors or LCoS projectors. As for color-framing mechanism, one-chip DLP projectors use rotating color wheel or blinking trichromatic LEDs, and one-chip LCD projectors use the micro color filter array, which is similar to the Bayer pattern in RGB cameras. By using the color-framing mechanism of a one-chip DLP projector, Ashdown et al. [4] recovered high-resolution spectral reflectance. Further, to deal with unexpected irregularities when applying a digital projector in non-ideal situations, they proposed to generate a compensation image based on both radiometric model of system and the content

of the image. Tanaka et al. [33] utilized a projector coaxially placed with the camera to inject illuminations of multiple frequencies for obtaining the appearance of individual inner slices. Projectors have also been used for adversarial attacks in physical world with projected perturbations [14] or constant colors [18].

Existing polarization-based LCD/LCoS projectors do not offer pixel-wise manipulation of the polarization status of light projected on the screen. So, they can not be directly utilized to attack polarization-based vision algorithms. In the following, we will show that a simple adaptation of the one-chip LCD projector will allow locally controllable polarizing projection.

3. Locally Controllable Polarizing Projection

3.1. Principle of One-chip LCD Projector

One-chip LCD projector is the most widely used type of low-cost projector. The principle of an LCD projector controlling the irradiance is shown in Figure 2. A beam of unpolarized light is emitted by a bulb. Two linear polarizers are placed in coaxial positions while their polarizing directions are perpendicular to each other ($\frac{3\pi}{4}$ and $\frac{\pi}{4}$ in our device), and a liquid crystal panel is inserted to the middle of them. The light is divided into red, green, and blue components by a color filter array before linearly polarized by the back $\frac{3\pi}{4}$ polarizer. Then, by adding voltages to liquid crystal grids, the layer can manipulate polarizing direction of individual light beams, and a greater voltage leads to a bigger rotation up to $\frac{\pi}{2}$ from its initial direction. The light's intensity passing through the front polarizer is decided by its polarizing direction, following the Malus's law:

$$I = I_0 \cos^2(\theta), \quad (1)$$

where θ is the angle between the polarizing direction of light after being rotated by the liquid crystal and direction of the front $\frac{\pi}{4}$ polarizer. I_0 is a constant light intensity from the back polarizer. Since the intensity of RGB components is separately controlled, the color of merged light can be manipulated to match the projection pattern sufficiently.

Note that, with the front polarizer equipped, output light beams are always linearly polarized in the $\frac{\pi}{4}$ axis related to the projector but have different intensities, as shown in Figure 3 (c). *The key idea of building a controllable polarization light projector is to remove the front polarizer.* As shown in the Figure 3 (a,b), we tear off the front polarization film of the projector, and manage not to damage the liquid crystal panel. In this way, output lights of the projector have constant intensity but different polarizing directions. The polarizing direction can be precisely controlled by manipulating the projection pattern. Furthermore, uniform white color and constant projection intensity contribute to high

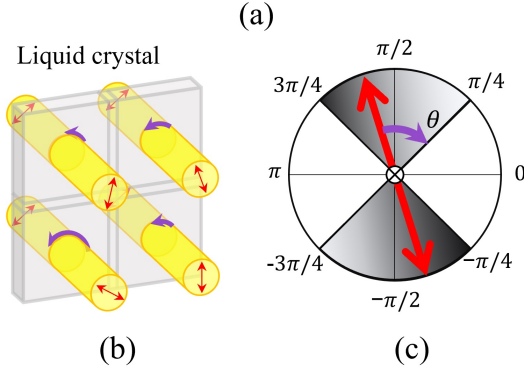
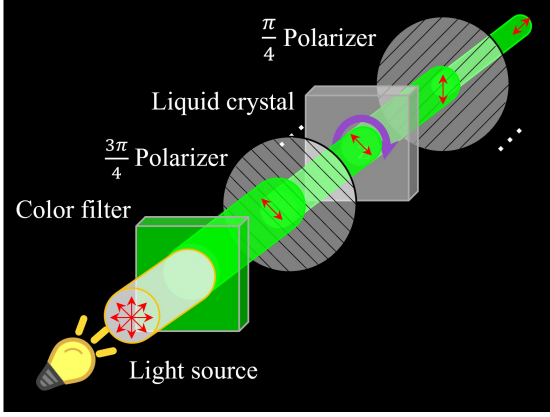


Figure 2. (a) The mechanism of intensity adjustment in one-chip LCD projector with a liquid crystal panel sandwiched by two perpendicular linear polarizers. (b) The polarization direction of light beam in each liquid crystal cell can be individually controlled, without affecting its intensity. (c) The range of controllable polarization direction.

stealthiness as it will not introduce visible textures to human eyes, as can be seen in Figure 3 (d).

4. Preliminaries for Light Polarization

Most polar-RGB based methods rely on both intensity and polarization cues, i.e., degree of linear polarization (DoLP, ρ , the proportion of linear polarized component in light) and angle of linear Polarization (AoLP, ϕ , the polarizing direction of polarized light). They can be calculated from a single shot with a Bayer-polarization sensor, e.g., IMX250MYR, which captures polarization components in four directions, termed as I_0 , $I_{\pi/4}$, $I_{\pi/2}$, and $I_{3\pi/4}$. Stokes vector, $\mathbf{S} = [S_0, S_1, S_2, S_3]^T$ is used to describe the polarization state of light, where S_0 represents the total intensity of light, S_1 and S_2 describe the polarization states in horizontal and diagonal axes, and S_3 presents circular polarization.

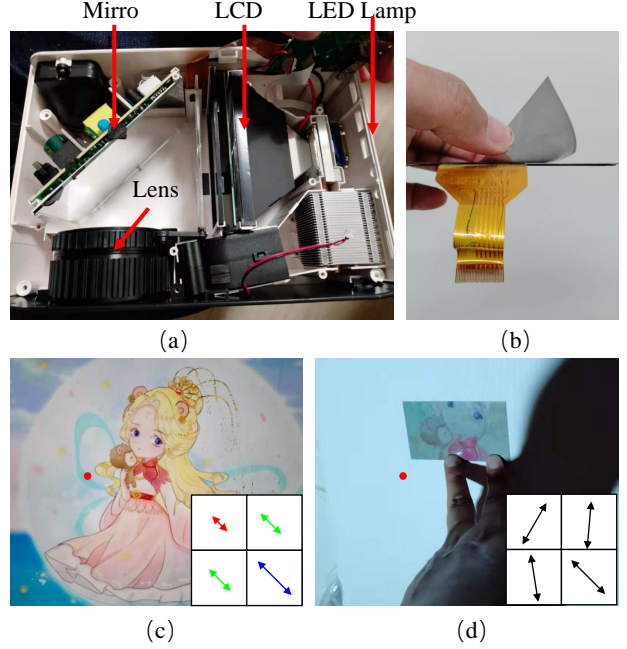


Figure 3. (a) The typical structure of a one-chip LCD projector, in which light emitted by LED lamp will go through liquid crystal panel, mirror, and projection lens. (b) A linear polarizer is attached on the front side of the LCD panel. We tear it off to make our polarizing projection for adversarial attacks. (c)(d) The projection of a normal LCD projector and our adapted projector. The arrows' direction and length represent polarizing direction and intensity, respectively. A normal projector emits out colorful light of constant polarization direction, while our adapted polarizing projector emits light with constant intensity but different polarizing angles. Note that, for naked eyes and ordinary RGB cameras, the projected light is completely uniform, even if their polarization directions are totally different. The projected image can be observed by eyes with the assistance of a linear polarizer on the screen.

S_0 , S_1 and S_2 can be computed following:

$$\begin{aligned} S_0 &= \frac{(I_0 + I_{\pi/4} + I_{\pi/2} + I_{3\pi/4})}{2} \\ S_1 &= I_0 - I_{\pi/2} \\ S_2 &= I_{\pi/4} - I_{3\pi/4}. \end{aligned} \quad (2)$$

Note that integration of multiple light can be calculated as linear combination of their Stokes parameters. Then, ρ and ϕ are generated by Stokes elements as:

$$\rho = \frac{\sqrt{S_1^2 + S_2^2}}{S_0}, \phi = \frac{1}{2} \arctan \frac{S_2}{S_1}. \quad (3)$$

Also, S_1 and S_2 can be computed from S_0 , ρ and ϕ by:

$$S_1 = S_0 \rho \cos(2\phi), S_2 = S_0 \rho \sin(2\phi). \quad (4)$$

5. Whitebox Attack on Glass Segmentation

Based on the novel locally controllable polarizing projection, we will show how to attack a polar-RGB based AI model, PGSNet for glass segmentation [27], mainly in a whitebox manner. Assuming full access to the target model, our goal is to design an effective attack setting, find a stable perturbation, and project it onto targeted scene in physical world. The projected adversarial attacker will NOT be recognized by human eyes, since it appears to be uniform white, yet can be captured by a polar-rgb camera. The PGSNet model with manipulated input will generate wrong predictions.

5.1. Our Setting’s Challenges

Fine-scaled perturbations like pixel-wise noises are extremely subtle and easy to be destroyed in complicated physical world. Therefore, previous works apply large perturbation patterns, like blocks [12], lines [11], triangles [40], for attacking image classification models. However, segmentation models predict pixel-wise classifications, which also apply advanced multiscale architectures, skip connections, and even self-attention modules, making them robust to adversarial attacks [3, 21]. Thus, we develop a perturbation pattern in the form of regular grids, and all elements in each grid cell are broadcasted with a shared perturbation value, to realize more robust physical attack.

Normally, whitebox adversarial attacks in physical world need to simulate comprehensive effects in real world, including camera response function, camera noises, light decay, quantization effects, and so on [14, 20]. Therefore, in order to attack a polarization-based AI model, the most proper way of generating an effective perturbation in the whitebox manner is to simulate the complete transport of light. For us, polarization light travels from the polarizing projector to the object’s surface, and finally to the polarization camera after being reflected by the object. However, as far as we know, there does not exist any method to acquire accurate pBRDF parameters in the wild. So, we consider a simplified setup for whitebox attacks on glass segmentation. We can not only construct the most reliable simulation for polarization projection on glasses in digital world, but also generate adversarial examples of high effectiveness in the physical world.

5.2. Digital World Attack

Given a set of clean inputs S_b in the form of Stokes vector and its binary label $y \in \mathbb{R}^{H \times W \times 1}$, where (H, W) denotes spatial resolution. PGSNet $f(\cdot)$ is trained to maximize the pixel-wise binary prediction accuracy, where 1/0 represent the region is/is not glass. The goal of our adversarial attack is to maximize the segmentation error with a projected adversarial perturbation, denoted as S in the form

of Stokes vector. The problem is then formulated as

$$\max_S \frac{1}{HW} \|y - f(g(S_b + S))\|, \quad (5)$$

where $g(\cdot)$ denotes mapping from Stokes vectors to polarization cues.

In general, adversarial attack algorithms generate adversarial examples following the negative gradient direction and the perturbation is the division of clean image and its adversarial optimization result. However, perturbation generated in this approach does not obey physical property of our polarizing projection. For an optical adversarial system, we need to update perturbation directly on the perturbation [14], i.e., the projection pattern that will be fed into the projector in our setting.

To narrow down the gap between the digital world and physical world, we generate our adversarial example from a collection of real-world polarization images, termed as $S_i \in \mathbf{S}_p = \{S_1, S_2, \dots, S_K\}$, captured directly by the targeted camera in the scene covered by the corresponding constant projections $v_i \in \mathbf{v}_p = \{v_1, v_2, \dots, v_K\}$. The background without projection is also captured as S_b . While our projected perturbation is a map of grids, the value of each grid is assigned with a selected value \hat{v}_i . With the relationship between the reflection S_i and the quantized projection v_i known, we can realize optimization using \mathbf{S}_b rather than \mathbf{v}_b to avoid direct simulation of polarization reflection effects as well as tone-mapping curve of the projector.

To get the most effective adversarial perturbation for each grid in an optimization-based approach, we hold a set of optimizable weights $\omega_i \in \Omega = \{\omega_1, \omega_2, \dots, \omega_K\}$ on candidate images and use *SoftMax* function to generate relative coefficients of each S_i . Then we compute an adversarial example as:

$$S_{ae} = \sum_i^K \frac{\exp(\omega_i/\tau)}{\sum_j^K \exp(\omega_j/\tau)} (S_i - S_b) + S_b^*, \quad (6)$$

with original environment illuminations subtracted and further modified to S_b^* if needed. τ is a temperature parameter to adjust the bias of relative weights. We set τ as 0.2 for a simulation closer to captured real world images. The weights ω_i is our main optimization target for generating a perturbation from the real world set \mathbf{S}_p . For a grid, the problem in equation 5 is then reformulated as:

$$\max_{\Omega} \frac{1}{N} \|y - f(g(S_{ae}))\|, \quad (7)$$

where N counts for the amount of pixels.

To deal with the problem in equation 7, we follow the negative gradient directions to update Ω based on an iterative optimization approach:

$$\Omega^{t+1} \leftarrow \Omega^t + \alpha \nabla_{\Omega} L(y, f(g(S_{ae}))), \quad (8)$$

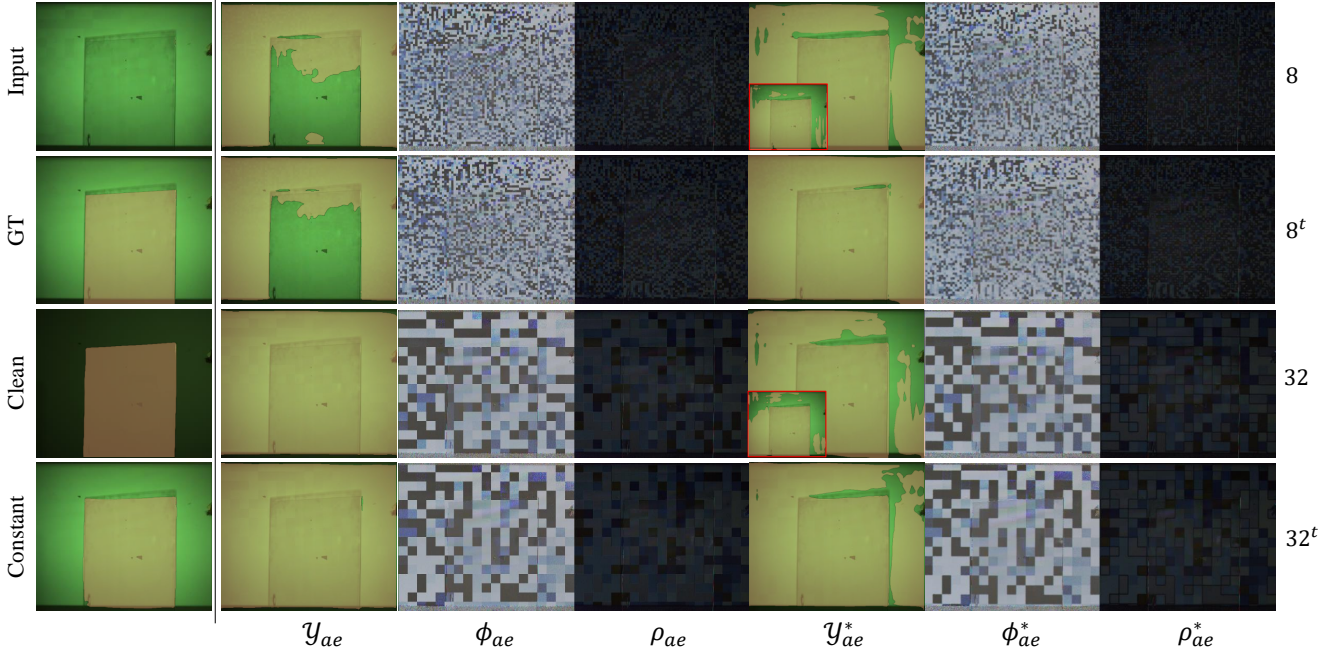


Figure 4. Visual comparison for adversarial attacks on the polarization-based glass segmentation model PGSNet [27]. y_{ae} , ϕ_{ae} and ρ_{ae} present predictions, AoLP, and DoLP of adversarial examples, and * denote experiments in the physical world. The orange denotes regions predicted as glass pixels. 8 and 32 represent grid sizes and t denotes perturbations generated with EOT. The sub-pictures in red square show predictions with randomly generated perturbations.

where α denotes the step size. After the optimization, we use $ArgMax$ function to decide the final $\hat{\Omega}$ to form an adversarial perturbation. In practice, we collected a set of candidate images consisting of 9 images projected by the polarization projections whose source projection values are known and uniformly discrete. Please refer to our supplementary material for more details.

5.3. Adversarial Loss

With our adversarial example, we aim to maximize the error between predicted glass segmentation map $f(g(S_{ae}))$ and label y , thus we firstly apply a Binary Cross Entropy loss. Moreover, we prefer to mislead the PGSNet to predict more negative pixels to be positive, and on the oppsite predict more positive pixels to negative as in [17]. Thus our final adversarial loss function is

$$\mathcal{L} = \mathcal{L}_{BCE} + \lambda \mathcal{L}_E. \quad (9)$$

Please refer to our supplementary for more details.

5.4. Physical world attack

To generate more robust adversarial examples, we follow the data augmentation strategy of EOT (Expectation Over Transformation) [5]. EOT employs a distribution of real world degradations and transformations to generate adversarial examples fit to complicated physical world. As we only consider a constrained setting of fixed known camera

and projector, transformations like rotation and translation are out of our concerns. We add Gaussian noises and Gaussian blur for handling real world degradation and further use a randomly sampled scale ratio to re-scale S_b , which counts for small alters in background illuminations.

5.5. Experiments

To further simplify our experiments, we apply a specific setting of co-located projector and camera that we can eliminate the calibration process of their relative poses and easily align the view of camera and the projection. We collect candidate images as well as a background image in an indoor scene. Digital world attacks are conducted and the generated adversarial projection perturbations are applied in physical world attacks. The results are shown in Figure 4.

We illustrate adversarial results of two grid sizes, 8 and 32. Compared to predictions with the background image (Clean) and the scene illuminated by projection of constant polarization (Constant), the predictions $y_{ae}^{(*)}$ (* for physical world attacks) show effectiveness of our estimated adversarial perturbations on misleading PGSNet in both digital world and physical world. The attacks successfully lead to opposite predictions in digital world with a perturbation of a higher resolution (block size 8), and fail its recognition in all scenarios.

Specifically, the input image as shown in Figure 4 validates that our adversarial polarization projections achieve

Table 1. Quantitative comparison of adversarial examples in IoU and BER in the digital and physical world. The numbers denote block size, ran. present randomly sampled perturbation, and t denote perturbations generated with EOT.

	Digital world		Physical world	
	IoU ↓	BER ↑	IoU ↓	BER ↑
Clean	0.957	1.61	0.957	1.61
8 ran.	0.571	23.59	0.584	22.58
8	0.001	98.17	0.437	40.72
8 ^t	0.006	95.81	0.379	50.95
16 ran.	0.432	41.09	0.405	46.48
16	0.378	50.47	0.404	46.63
16 ^t	0.385	49.5	0.385	49.50
32 ran.	0.435	40.68	0.596	21.52
32	0.382	50.23	0.469	35.58
32 ^t	0.382	50.08	0.414	43.99

adversarial attacks within the domain of polarization. While few visual textures are introduced to human eyes, the polarization property is completely modified with our perturbation projections. AoLP and DoLP of digital world simulation and physical world capturing show that our simulation approach reconstructs realistic polarization reflections at an extremely high precision. We successfully directly attack the polarization cues of the targeted model, achieving effectiveness and stealthiness at the same time.

Quantitative evaluations are shown in Table 1. The comparison indicates that with a higher resolution, an adversarial perturbation achieves a higher attack performance in our indoor scene. Further, EOT is capable to improve adversarial examples’ transferability to physical world. Last but not least, our optimized adversarial examples outperform randomly generated perturbations with a great margin. More experimental results are presented in our supplementary material.

6. Blackbox Attack on Color Constancy

The DoLP-based color constancy algorithm [30] relies on polarization properties of reflections to infer the global illumination. The algorithm uses DoLP to search achromatic pixels within an image, whose reflection color directly reflects color of light source. For chromatic pixels, a robust prior knowledge and an assumption are applied, that their white-balanced color should be opposite to its DoLP color, and the AoLP of specular and diffuse reflection polarizing in orthogonal directions. For most lighting conditions in the wild, the assumption is well grounded as illuminations of non-polarization or low-polarization dominate, and global illuminations generally convey limited intensity caused by reflections from other objects or inter-reflections. However, our polarizing projection is capable of emitting linearly polarized light through separate color

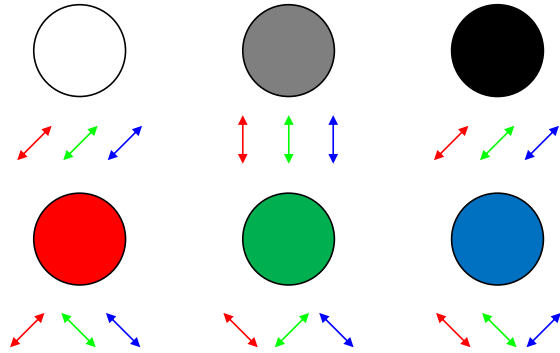


Figure 5. Illustration of projections and their corresponding color-wise polarization directions. The arrows illustrate color-wise linear polarization emissions polarized in the x-y plane of projector’s coordinate and transport forward.

channels, which is able to destroy their assumption.

As the algorithm utilizes simple statistic computation to estimate a global lighting ratio, we believe an intuitive yet effective way can destroy the color constancy algorithm in a blackbox attack manner, by simply projecting colors of three channels in different polarizing directions. To evaluate it, we apply several simple projection settings. By projecting specific color values, the polarizing direction of three color channels are shown in Figure 5. While diffuse polarization is barely influenced by polarization state of incident light, specular reflections well retain linearity of incident light.

Figure 6 exhibits restored images with estimated white-balance ratios under scenes dominated by our polarizing projections. The reflections are dominated by specular reflections. The labels illustrate the related color to the projection polarization direction as in Figure 5, and DoLP and AoLP are ranged to color space in the order of R, G, B. The results illustrate that while reflections have greater DoLP in, e.g., blue and green, the algorithm is fooled to estimate cyan illumination and enhance the red channel, as shown in Figure 6 Red. Further, the AoLP maps are modified with significant color biases regarding to the polarization projections, which could lower credibility of their AoLP-based ambient light identification.

We also take experiments in a scene containing more diffuse regions, as shown in Figure 7. Since the target algorithm can handle colorful illuminations, we use additional color filters placed onto the lens to create non-white illuminations. As shown in the figure, the color filters can obstruct parts of illuminations, that color-wise polarization values are further modified. The results indicate that in such a diffuse-dominated scene, our polarization-based attack still achieves high effectiveness.

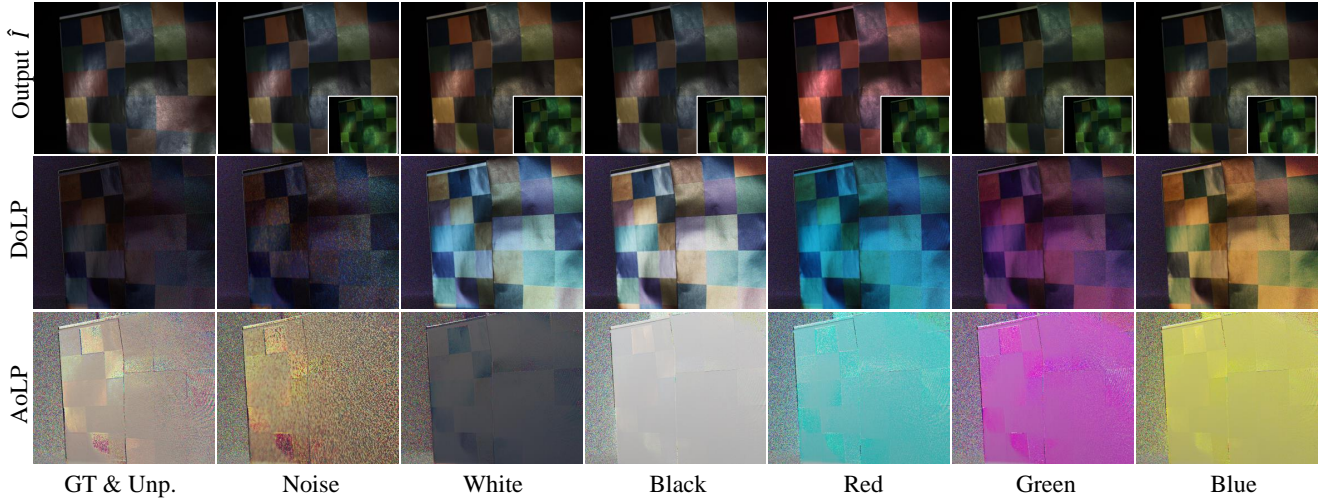


Figure 6. Color constancy results and visualizations of DoLP, AoLP under different color-wise polarization projections. Notice that our projection is always constant white light, the color labels only relate to color-wise polarizing directions as shown in Figure 5, but not real colorful projections.

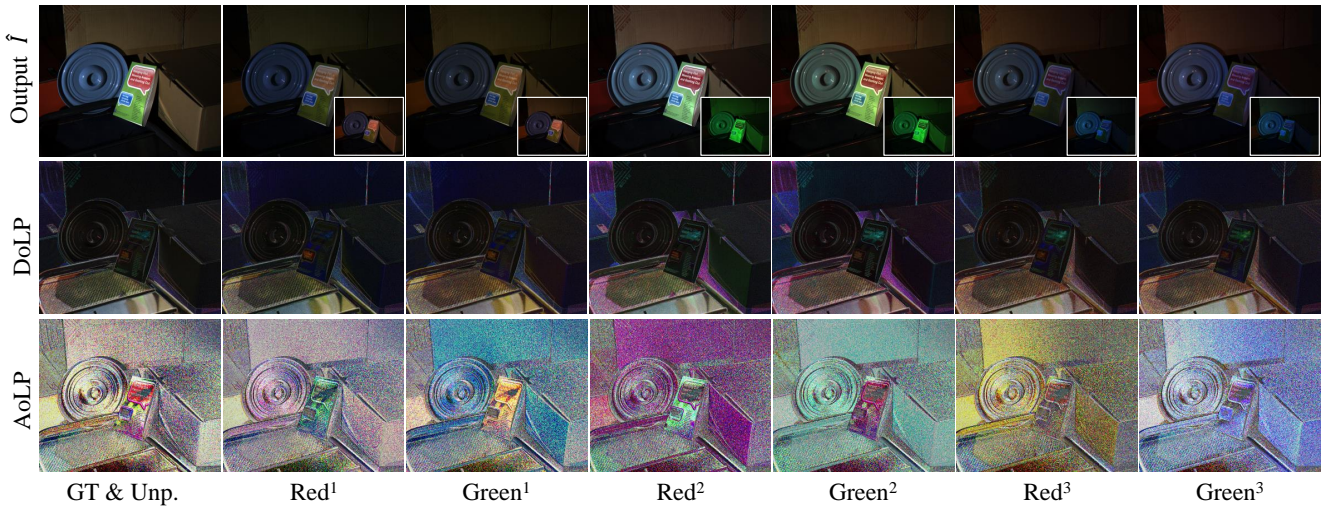


Figure 7. Color constancy results and visualizations of DoLP, AoLP under different color-wise polarization projections relating to Figure 5 through additional color filters placed in front of the lens (termed as superscripts $\{1,2,3\}$). The sub-picture at the bottom right corner shows the input images.

7. Research Ethics and Limitations

This study originates from our curiosity on the potential vulnerability of polarization-based vision algorithms in the digital space. In line with existing researches on adversarial attacks, this study is intended to offer a timely warning on the potential vulnerability of polarization-based AI.

The most obvious limitation we found lies in the relative low luminance of the projector, and the attack success rate will be low in bright environment. However, it is highly effective in indoor or low-light outdoor scenarios. Further protection measures, such as adversarial training and data enhancement, should be considered immediately.

8. Conclusion

Polarization has been utilized for a variety of computer vision tasks. We have shown that, similar to the well-known vulnerability of RGB-based vision, the performance of polarization-based vision algorithms, such as color constancy and glass segmentation, can be manipulated, maybe in a potentially harmful way. Our adversarial attackers are physically realized by using an adapted one-chip LCD projector, which allows locally controllable polarizing projection. Our method is visually friendly, thus poses realistic concerns on the reliability of polarization-based AI. We hope this study will arouse attentions on the potential risks of polarization-based vision.

References

- [1] Naveed Akhtar and Navid Kardan. Threat of adversarial attacks on deep learning in computer vision: A survey. *IEEE Access*, 6:14410–14430, 2018. [1](#)
- [2] Naveed Akhtar, Ajmal Mian, Navid Kardan, and Mubarak Shah. Advances in adversarial attacks and defenses in computer vision: A survey. *IEEE Access*, 9:155161–155196, 2021. [1](#)
- [3] Anurag Arnab, Ondrej Miksik, and Philip HS Torr. On the robustness of semantic segmentation models to adversarial attacks. In *Proceedings of the IEEE Conference on Computer Vision and Pattern Recognition*, pages 888–897, 2018. [5](#)
- [4] Mark Ashdown, Takahiro Okabe, Imari Sato, and Yoichi Sato. Robust content-dependent photometric projector compensation. In *2006 Conference on Computer Vision and Pattern Recognition Workshop (CVPRW'06)*, pages 6–6. IEEE, 2006. [3](#)
- [5] Anish Athalye, Logan Engstrom, Andrew Ilyas, and Kevin Kwok. Synthesizing robust adversarial examples. In *International conference on machine learning*, pages 284–293. PMLR, 2018. [2](#), [6](#)
- [6] Yunhao Ba, Alex Gilbert, Franklin Wang, Jinfa Yang, Rui Chen, Yiqin Wang, Lei Yan, Boxin Shi, and Achuta Kadambi. Deep shape from polarization. In *Computer Vision–ECCV 2020: 16th European Conference, Glasgow, UK, August 23–28, 2020, Proceedings, Part XXIV 16*, pages 554–571. Springer, 2020. [3](#)
- [7] Seung-Hwan Baek, Daniel S Jeon, Xin Tong, and Min H Kim. Simultaneous acquisition of polarimetric svbrdf and normals. *ACM Trans. Graph.*, 37(6):268–1, 2018. [3](#)
- [8] Nicholas Carlini and David Wagner. Towards evaluating the robustness of neural networks. In *2017 IEEE Symposium on Security and Privacy (SP)*, pages 39–57. Ieee, 2017. [2](#)
- [9] Zhaopeng Cui, Jinwei Gu, Boxin Shi, Ping Tan, and Jan Kautz. Polarimetric multi-view stereo. In *Proceedings of the IEEE conference on computer vision and pattern recognition*, pages 1558–1567, 2017. [3](#)
- [10] Valentin Deschaintre, Yiming Lin, and Abhijeet Ghosh. Deep polarization imaging for 3d shape and svbrdf acquisition. In *Proceedings of the IEEE/CVF Conference on Computer Vision and Pattern Recognition*, pages 15567–15576, 2021. [1](#), [3](#)
- [11] Ranjie Duan, Xiaofeng Mao, A Kai Qin, Yuefeng Chen, Shaokai Ye, Yuan He, and Yun Yang. Adversarial laser beam: Effective physical-world attack to dnns in a blink. In *Proceedings of the IEEE/CVF Conference on Computer Vision and Pattern Recognition*, pages 16062–16071, 2021. [2](#), [5](#)
- [12] Kevin Eykholt, Ivan Evtimov, Earlene Fernandes, Bo Li, Amir Rahmati, Chaowei Xiao, Atul Prakash, Tadayoshi Kohno, and Dawn Song. Robust physical-world attacks on deep learning visual classification. In *Proceedings of the IEEE conference on computer vision and pattern recognition*, pages 1625–1634, 2018. [5](#)
- [13] Yoshiki Fukao, Ryo Kawahara, Shohei Nobuhara, and Ko Nishino. Polarimetric normal stereo. In *Proceedings of the IEEE/CVF Conference on Computer Vision and Pattern Recognition*, pages 682–690, 2021. [1](#), [3](#)
- [14] Abhiram Gnanasambandam, Alex M Sherman, and Stanley H Chan. Optical adversarial attack. In *Proceedings of the IEEE/CVF International Conference on Computer Vision*, pages 92–101, 2021. [2](#), [3](#), [5](#)
- [15] Ian J Goodfellow, Jonathon Shlens, and Christian Szegedy. Explaining and harnessing adversarial examples. *arXiv preprint arXiv:1412.6572*, 2014. [2](#)
- [16] Jindong Gu, Hengshuang Zhao, Volker Tresp, and Philip Torr. Adversarial examples on segmentation models can be easy to transfer. *arXiv preprint arXiv:2111.11368*, 2021. [2](#)
- [17] Jindong Gu, Hengshuang Zhao, Volker Tresp, and Philip HS Torr. Segpgd: An effective and efficient adversarial attack for evaluating and boosting segmentation robustness. In *Computer Vision–ECCV 2022: 17th European Conference, Tel Aviv, Israel, October 23–27, 2022, Proceedings, Part XXIX*, pages 308–325. Springer, 2022. [6](#)
- [18] Chengyin Hu and Weiwen Shi. Adversarial color projection: A projector-based physical attack to dnns. *arXiv preprint arXiv:2209.09652*, 2022. [3](#)
- [19] Inseung Hwang, Daniel S Jeon, Adolfo Munoz, Diego Gutierrez, Xin Tong, and Min H Kim. Sparse ellipsometry: portable acquisition of polarimetric svbrdf and shape with unstructured flash photography. *ACM Transactions on Graphics (TOG)*, 41(4):1–14, 2022. [3](#)
- [20] Steve TK Jan, Joseph Messou, Yen-Chen Lin, Jia-Bin Huang, and Gang Wang. Connecting the digital and physical world: Improving the robustness of adversarial attacks. In *Proceedings of the AAAI Conference on Artificial Intelligence*, volume 33, pages 962–969, 2019. [2](#), [5](#)
- [21] Christoph Kamann and Carsten Rother. Benchmarking the robustness of semantic segmentation models. In *Proceedings of the IEEE/CVF conference on computer vision and pattern recognition*, pages 8828–8838, 2020. [5](#)
- [22] Alexey Kurakin, Ian J Goodfellow, and Samy Bengio. Adversarial examples in the physical world. In *Artificial intelligence safety and security*, pages 99–112. Chapman and Hall/CRC, 2018. [2](#)
- [23] Chenyang Lei, Xuhua Huang, Mengdi Zhang, Qiong Yan, Wenxiu Sun, and Qifeng Chen. Polarized reflection removal with perfect alignment in the wild. In *Proceedings of the IEEE/CVF Conference on Computer Vision and Pattern Recognition*, pages 1750–1758, 2020. [1](#), [3](#)
- [24] Chenyang Lei, Chenyang Qi, Jiaxin Xie, Na Fan, Vladlen Koltun, and Qifeng Chen. Shape from polarization for complex scenes in the wild. In *Proceedings of the IEEE/CVF Conference on Computer Vision and Pattern Recognition*, pages 12632–12641, 2022. [3](#)
- [25] Mengke Li, Naifu Yao, Sha Liu, Shouqing Li, Yongqiang Zhao, and Seong G Kong. Multisensor image fusion for automated detection of defects in printed circuit boards. *IEEE Sensors Journal*, 21(20):23390–23399, 2021. [1](#)
- [26] Aleksander Madry, Aleksandar Makelov, Ludwig Schmidt, Dimitris Tsipras, and Adrian Vladu. Towards deep learning models resistant to adversarial attacks. *arXiv preprint arXiv:1706.06083*, 2017. [2](#)

- [27] Haiyang Mei, Bo Dong, Wen Dong, Jiayi Yang, Seung-Hwan Baek, Felix Heide, Pieter Peers, Xiaopeng Wei, and Xin Yang. Glass segmentation using intensity and spectral polarization cues. In *Proceedings of the IEEE/CVF Conference on Computer Vision and Pattern Recognition*, pages 12622–12631, 2022. [1](#), [2](#), [3](#), [5](#), [6](#)
- [28] Shao Mingqi, Xia Chongkun, Yang Zhendong, Huang Junnan, and Wang Xueqian. Transparent shape from single polarization images. *arXiv preprint arXiv:2204.06331*, 2022. [3](#)
- [29] Seyed-Mohsen Moosavi-Dezfooli, Alhussein Fawzi, Omar Fawzi, and Pascal Frossard. Universal adversarial perturbations. In *Proceedings of the IEEE conference on computer vision and pattern recognition*, pages 1765–1773, 2017. [2](#)
- [30] Taishi Ono, Yuhi Kondo, Legong Sun, Teppei Kurita, and Yusuke Moriuchi. Degree-of-linear-polarization-based color constancy. In *Proceedings of the IEEE/CVF Conference on Computer Vision and Pattern Recognition*, pages 19740–19749. IEEE, 2022. [1](#), [2](#), [3](#), [7](#)
- [31] Mahmood Sharif, Sruti Bhagavatula, Lujo Bauer, and Michael K Reiter. Accessorize to a crime: Real and stealthy attacks on state-of-the-art face recognition. In *Proceedings of the 2016 acm sigsac conference on computer and communications security*, pages 1528–1540, 2016. [2](#)
- [32] Christian Szegedy, Wojciech Zaremba, Ilya Sutskever, Joan Bruna, Dumitru Erhan, Ian Goodfellow, and Rob Fergus. Intriguing properties of neural networks. *arXiv preprint arXiv:1312.6199*, 2013. [1](#), [2](#)
- [33] Kenichiro Tanaka, Yasuhiro Mukaigawa, Hiroyuki Kubo, Yasuyuki Matsushita, and Yasushi Yagi. Recovering inner slices of translucent objects by multi-frequency illumination. In *Proceedings of the IEEE Conference on Computer Vision and Pattern Recognition*, pages 5464–5472, 2015. [3](#)
- [34] Silvia Tozza, Dizhong Zhu, William AP Smith, Ravi Ramamoorthi, and Edwin R Hancock. Uncalibrated, two source photo-polarimetric stereo. *IEEE Transactions on Pattern Analysis and Machine Intelligence*, 44(9):5747–5760, 2021. [3](#)
- [35] Hui Wei, Tang Hao, Xuemei Jia, Hanxun Yu, Zhubo Li, Zhixiang Wang, Shin’ichi Satoh, and Zheng Wang. Physical adversarial attack meets computer vision: A decade survey. *arXiv preprint arXiv:2209.15179*, 2022. [2](#)
- [36] Zuxuan Wu, Ser-Nam Lim, Larry S Davis, and Tom Goldstein. Making an invisibility cloak: Real world adversarial attacks on object detectors. In *Computer Vision–ECCV 2020: 16th European Conference, Glasgow, UK, August 23–28, 2020, Proceedings, Part IV 16*, pages 1–17. Springer, 2020. [2](#)
- [37] Kaidi Xu, Gaoyuan Zhang, Sijia Liu, Quanfu Fan, Mengshu Sun, Hongge Chen, Pin-Yu Chen, Yanzhi Wang, and Xue Lin. Adversarial t-shirt! evading person detectors in a physical world. In *Computer Vision–ECCV 2020: 16th European Conference, Glasgow, UK, August 23–28, 2020, Proceedings, Part V 16*, pages 665–681. Springer, 2020. [2](#)
- [38] Luwei Yang, Feitong Tan, Ao Li, Zhaopeng Cui, Yasutaka Furukawa, and Ping Tan. Polarimetric dense monocular slam. In *Proceedings of the IEEE conference on computer vision and pattern recognition*, pages 3857–3866, 2018. [3](#)
- [39] Jinyu Zhao, Yusuke Monno, and Masatoshi Okutomi. Polarimetric multi-view inverse rendering. *IEEE Transactions on Pattern Analysis and Machine Intelligence*, 2022. [3](#)
- [40] Yiqi Zhong, Xianming Liu, Deming Zhai, Junjun Jiang, and Xiangyang Ji. Shadows can be dangerous: Stealthy and effective physical-world adversarial attack by natural phenomenon. In *Proceedings of the IEEE/CVF Conference on Computer Vision and Pattern Recognition*, pages 15345–15354, 2022. [2](#), [5](#)

Fooling Polarization-based Vision using Locally Controllable Polarizing Projection

Supplementary Material

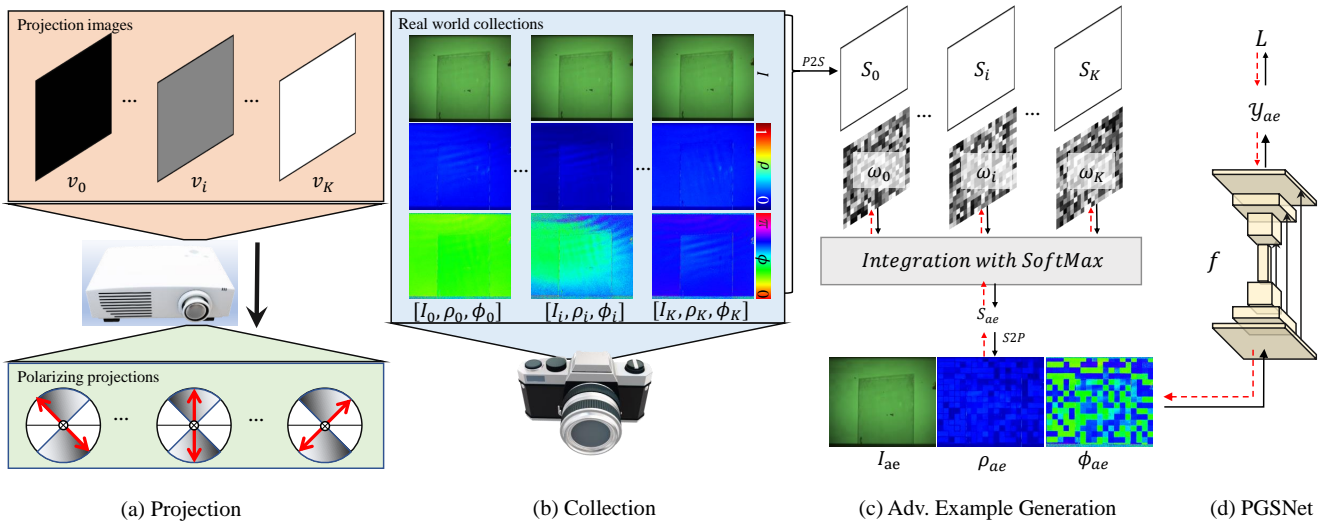


Figure 1. Illustrations of (a) polarizing projections, (b) candidate images collection, (c) adversarial example generation, and (d) feed forward & gradient backward of the polarization-RGB-based glass segmentation model PGSNet [6]. v_i represents the pixel value for the projected monochromatic image. $[I_i, \rho_i, \phi_i]$ denote captured polarization cues, including intensity, DoLP, and AoLP maps, and S_i are the same data in the form of Stokes parameters. $S2P$ and $P2S$ represent conversions between Polarization cues and Stokes parameters. Black and red dashed lines in (c), (d) counts for flows of data feed-forward and gradients backward propagation.

1. Whitebox Attack on Glass Segmentation

1.1. Implementation Details

We propose to employ locally controllable polarizing projection to fool the polarization-RGB-based glass segmentation model, PGSNet [6], in the physical world. We control the polarizing projection by projecting specific images according to the principle of our adapted one-chip LCD projector. In general, physical world adversarial attacks require realistic simulations of targeted objects as well as scenes injected with adversarial perturbations, *e.g.*, projection [4], shadow [8], and stickers [3], to search a robust and effective adversarial perturbation pattern. However, polarization reflection modeling requires accurate pBRDF parameters [2] and geometries that are unavailable in the wild. Thus, we propose a simplified approach for constructing a simulation of high precision.

Our perturbation is a map of grids, and pixels in each grid are assigned a same value to construct a perturbation robust enough to be captured in the complex real world. The adversarial perturbation should be estimated in an optimization-based approach in whitebox attack. To avoid physics-based simulation of polarized light transports from the projector to the camera, which involves the non-linear function of the projector and polarization reflection modeling, we generate adversarial examples from a set of candidate real captures whose projection values are known.

Concretely, we first set the projector (ELEPHAS W13 after hardware modification) and RGB-P camera (BFS-U3-51S5PC-C equipped with the IMX250MYR Polar-RGB sensor) in the same place and both look forward to the target scene. Then, we project flat grayscale images of a gray level $\{v_0, \dots, v_K\}$ uniformly sampled from 0 to 255, which causes projections with constant polarizing directions, as

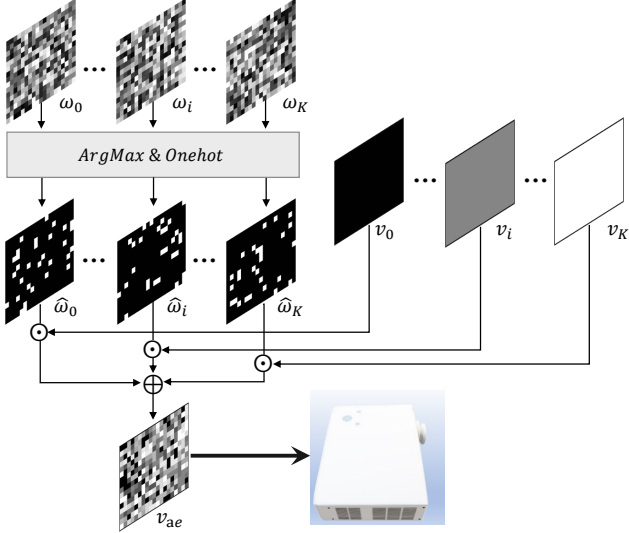


Figure 2. The illustration of generating final projection perturbation image. The optimized weights $\Omega = \{\omega_0, \dots, \omega_K\}$ is processed by the *ArgMax* function and converted into one-hot maps as $\hat{\omega}_i$, and finally integrated into the ultimate projection perturbation image v_{ae} .

shown in Figure 1 (a). Next, we capture a sequence of real-world images as a set of bases. As shown in Figure 1 (b) in the form of polarization cues, in contrast to few differences between the intensity images I_i , their AoLP maps ϕ_i are significantly changed by polarizing projections. In Figure 1 (c), the basis images in the form of Stokes parameters are integrated into S_{ae} with a set of optimizable weight maps $\Omega = \{\omega_0, \dots, \omega_{pk}\}$ through the *SoftMax* function as:

$$S_{ae} = \sum_i^K \frac{\exp(\omega_i/\tau)}{\sum_j^K \exp(\omega_j/\tau)} (S_i - S_b) + S_b^*, \quad (1)$$

where S_b denotes the Stokes parameter of background and S_b^* is that rescaled for augmentation. The integration $[I_{ae}, \rho_{ae}, \phi_{ae}]$ is fed into PGSNet as an adversarial example, to optimize the coefficient maps Ω , as shown in Figure 1 (d).

After the optimization, the best projection value in each grid is selected from $\{v_0, \dots, v_K\}$ by *ArgMax* function. As shown in Figure 2, v_{ae} is our final perturbation image for polarizing projection. The proposed approach generates adversarial examples and optimizes the perturbation from real images, thus achieving high effectiveness in the physical world attack.

1.2. Adversarial Loss

The total loss function consists of a BCE loss and L_E . We want to mislead the PGSNet to predict more negative pixels to be positive, and on the opposite predict more positive pixels to be negative as [5]. Thus, with the prediction

of adversarial example y_{ae} , L_E is termed as:

$$\mathcal{L}_E = \frac{1}{HW} \sum_{j \in y^n} y_{ae}^j - \frac{1}{HW} \sum_{j \in y^p} y_{ae}^j, \quad (2)$$

where $y^{\{n,p\}}$ denotes the set of pixels which are negative / positive (not-glass / glass) in the label y . y^n and y^p are disjoint, and the total number of pixels of $y^n \cup y^p$ is HW .

1.3. Experiment

We show more visual results of physical world attacks. As shown in Figure 3, compared with unpolarized illumination (Unp.) or random perturbations (in the sub-pictures), our optimized polarizing projections achieve effective and robust adversarial attacks in the physical world. For scene 3 (a), random perturbation is sufficient to mislead the PGSNet while the background wall is glossy and the edge of the glass is not distinct enough. But randomly sampled perturbations fail in a more complicated scene (b), in which the glass has clear edges and prominent polarization cues. In contrast, our adversarial projection perturbation is optimized in a whitebox manner with simulating real-world degradations, thus can deal with such complex cases.

2. Blackbox Attack on Color Constancy

2.1. Implementation Details

The DoLP-based color constancy algorithm [7] estimates white-balance ratios from channel-wise polarization cues, DoLP principally. Thus, we simply project empty colorful images, which represent color-wise polarizing projections, to misguide the restoration. Note that, since our LCD projector has three (R, G, B) independent color channels, the polarization direction of each color channel can be controlled individually. We utilize this color-wise flexibility for fooling color constancy, with uniform value in each color channel of the projection image. As shown in Figure 4 (a), while we project an empty image filled with red ($[255, 0, 0]$ in 3 channels) to the target scene, our polarizing projector projects constant white light, of which RGB components are linearly polarized in individual directions. The original raw image I_{ori} in (a) is slightly green even under white illumination, since the automatic white balance mode of the camera is switched off. We can also employ an additional color filter before the projector to further modify the illumination color, as shown in Figure 4 (b), which usually makes color constancy more challenging.

References

- [1] Anish Athalye, Logan Engstrom, Andrew Ilyas, and Kevin Kwok. Synthesizing robust adversarial examples. In *International conference on machine learning*, pages 284–293. PMLR, 2018. 3

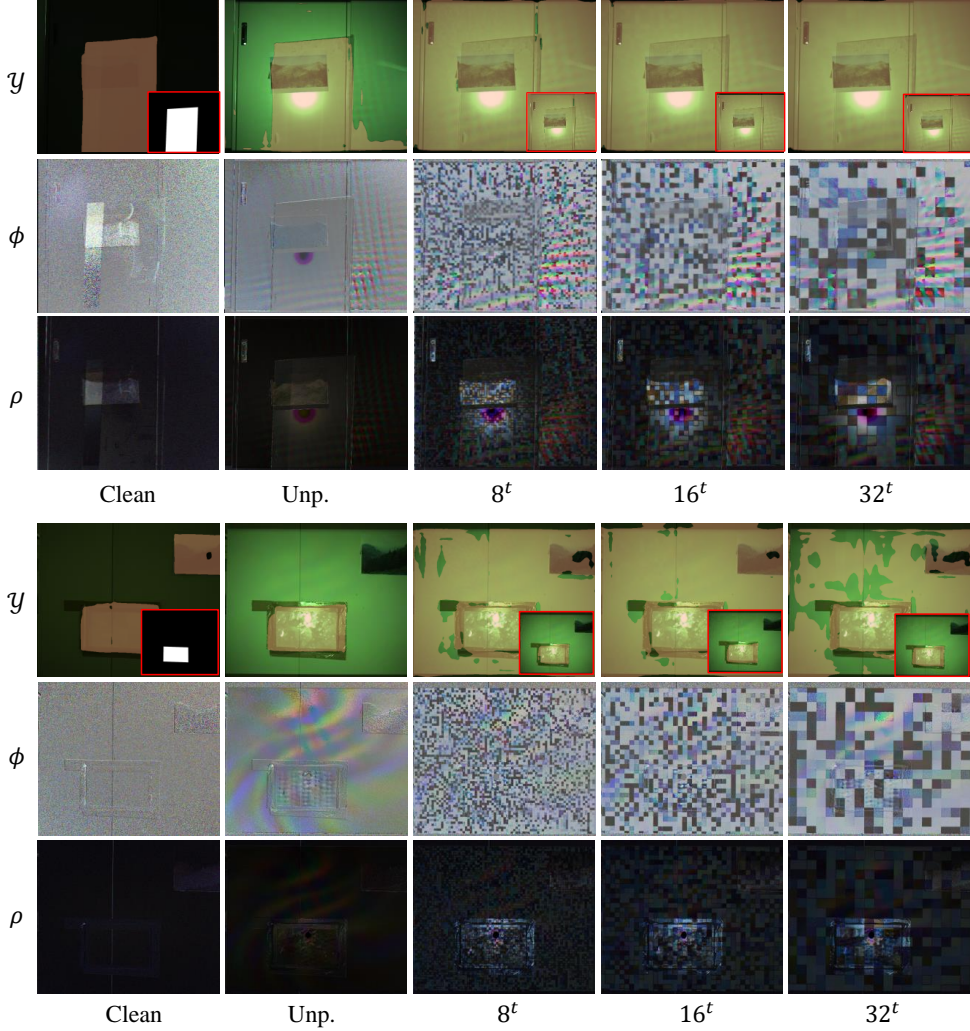


Figure 3. Visual comparisons for adversarial attacks on the polarization-based glass segmentation model PGSNet [6] in the physical world. y , ϕ and ρ represent predictions, AoLP, and DoLP maps respectively. The orange denotes regions predicted as glass pixels. Clean shows background images caused by environment lighting, without any projections. Unp. denotes scenes illuminated by unpolarized light. 8, 16 and 32 represent grid sizes and $*^t$ denotes perturbations optimized with simulated real-world disturbances [1]. The sub-pictures in red square in Clean show labels and the others show predictions with randomly generated perturbations in the corresponding grid sizes.

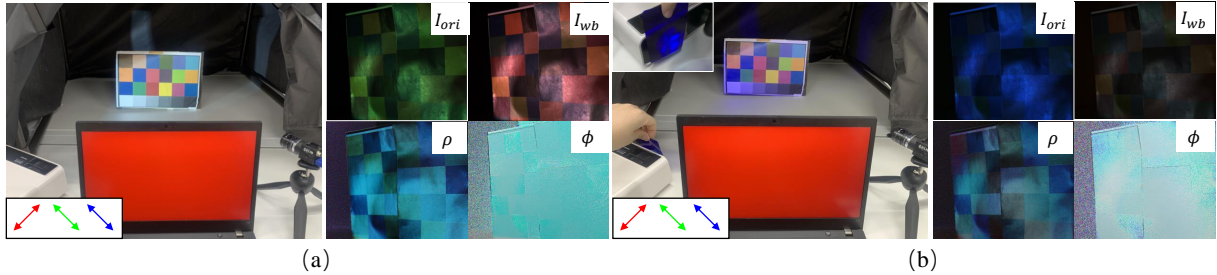


Figure 4. Illustrations for blackbox attacks on DoLP-based color constancy using color-wise polarizing projections. (a) and (b) are scenes w/o and w/ an additional color filter before the projector. The connected computer controls the polarizing projector by projecting an image, e.g., a red image. Note that, although the projection image is red, the projected light is uniform white to human eyes (a). After going through an additional blue filter, the light looks blueish to human eyes (b). The polarization direction of emitted color-wise polarizing projection is illustrated in the left-bottom in (a), (b). I_{ori} , ρ , ϕ are intensity, DoLP, and AoLP maps, and I_{wb} is the restoration result.

- [2] Seung-Hwan Baek, Daniel S Jeon, Xin Tong, and Min H Kim. Simultaneous acquisition of polarimetric svbrdf and normals. *ACM Trans. Graph.*, 37(6):268–1, 2018. [1](#)
- [3] Kevin Eykholt, Ivan Evtimov, Earlene Fernandes, Bo Li, Amir Rahmati, Chaowei Xiao, Atul Prakash, Tadayoshi Kohno, and Dawn Song. Robust physical-world attacks on deep learning visual classification. In *Proceedings of the IEEE conference on computer vision and pattern recognition*, pages 1625–1634, 2018. [1](#)
- [4] Abhiram Gnanasambandam, Alex M Sherman, and Stanley H Chan. Optical adversarial attack. In *Proceedings of the IEEE/CVF International Conference on Computer Vision*, pages 92–101, 2021. [1](#)
- [5] Jindong Gu, Hengshuang Zhao, Volker Tresp, and Philip HS Torr. Segpgd: An effective and efficient adversarial attack for evaluating and boosting segmentation robustness. In *Computer Vision–ECCV 2022: 17th European Conference, Tel Aviv, Israel, October 23–27, 2022, Proceedings, Part XXIX*, pages 308–325. Springer, 2022. [2](#)
- [6] Haiyang Mei, Bo Dong, Wen Dong, Jiaxi Yang, Seung-Hwan Baek, Felix Heide, Pieter Peers, Xiaopeng Wei, and Xin Yang. Glass segmentation using intensity and spectral polarization cues. In *Proceedings of the IEEE/CVF Conference on Computer Vision and Pattern Recognition*, pages 12622–12631, 2022. [1](#), [3](#)
- [7] Taishi Ono, Yuhi Kondo, Legong Sun, Teppei Kurita, and Yusuke Moriuchi. Degree-of-linear-polarization-based color constancy. In *Proceedings of the IEEE/CVF Conference on Computer Vision and Pattern Recognition*, pages 19740–19749. IEEE, 2022. [2](#)
- [8] Yiqi Zhong, Xianming Liu, Deming Zhai, Junjun Jiang, and Xiangyang Ji. Shadows can be dangerous: Stealthy and effective physical-world adversarial attack by natural phenomenon. In *Proceedings of the IEEE/CVF Conference on Computer Vision and Pattern Recognition*, pages 15345–15354, 2022. [1](#)